JOURNAL OF GEOPHYSICAL RESEARCH, VOL. 114, B04207, doi:10.1029/2008JB006219, 2009

Fallout and distribution of volcanic ash over Argentina following the May 2008 explosive eruption of Chaitén, Chile

Sebastian F. L. Watt,[1] David M. Pyle,[1] Tamsin A. Mather,[1] Robert S. Martin,[2] and Naomi E. Matthews[1]

Received 19 November 2008; revised 16 February 2009; accepted 28 February 2009; published 28 April 2009.

[1] The major explosive eruption of Chaitén volcano, Chile, in May 2008 provided a rare opportunity to track the long-range dispersal and deposition of fine volcanic ash. The eruption followed ~10,000 years of quiescence, was the largest explosive eruption globally since Hudson, Chile, in 1991, and was the first explosive rhyolitic eruption since Novarupta, Alaska, in 1912. Field examination of distal ashfall indicates that $\sim 1.6 \times 10^{11}$ kg of ash (dense rock equivalent volume of ~ 0.07 km^3) was deposited over $\sim 2 \times 10^5$ km^2 of Argentina during the first week of eruption. The minimum eruption magnitude, estimated from the mass of the tephra deposit, is 4.2. Several discrete ashfall units are identifiable from their distribution and grain size characteristics, with more energetic phases showing a bimodal size distribution and evidence of cloud aggregation processes. Ash chemistry was uniform throughout the early stages of eruption and is consistent with magma storage prior to eruption at depths of 3–6 km. Deposition of ash over a continental region allowed the tracking of eruption development and demonstrates the potential complexity of tephra dispersal from a single eruption, which in this case comprised several phases over a week-long period of intense activity.

Citation: Watt, S. F. L., D. M. Pyle, T. A. Mather, R. S. Martin, and N. E. Matthews (2009), Fallout and distribution of volcanic ash over Argentina following the May 2008 explosive eruption of Chaitén, Chile, *J. Geophys. Res.*, *114*, B04207, doi:10.1029/2008JB006219.

1. Introduction

[2] Chaitén, a southern Andean arc volcano (42.8°S), began erupting explosively on 2 May 2008, without recognized warning. Prior to this, the volcano comprised a rhyolitic lava dome within a 2.5 km diameter caldera, last thought to have erupted at 9370 ^{14}C years B.P. [*Naranjo and Stern*, 2004]. The event had immediate social and economic impacts across southern Chile and Argentina, with more than 5000 people evacuated from settlements up to 75 km from the volcano, and extensive ash deposition leading to regional disruption of agriculture and aviation.

[3] From examination of Moderate Resolution Imaging Spectroradiometer (MODIS; http://modis.gsfc.nasa.gov) satellite images and contemporary reports [*Folch et al.*, 2008], we produce the following summary of the early stages of the Chaitén eruption (Figure 1b). Activity was most vigorous during the first week of eruption, beginning with an energetic phase on 2 May, for which contemporary reports estimate a column height of 15 km. The plume from this episode was directed SE across the Andes, with sharp edges, before becoming more dispersed and drifting northward toward the Argentinean city of Bariloche (Figure 1b). This was followed by a sustained explosive phase, with a lower column height estimated to be 10 km or less, beginning on 3 May. This phase formed a continuous, linear, sharp-edged plume, moving SE and traveling beyond the Atlantic coast of Argentina. The intensity of this phase may have been variable, but by 5 May a similarly continuous, linear plume had an easterly orientation, with dispersed ash clouds reaching across the Atlantic ocean, and others drifting northward along the Atlantic coast of Argentina. On these images ash deposition is visible on the ground, with a dense gray coverage in the region around Esquel, arising from the 2 May phase, but no clear evidence of ground deposition as far as Bariloche. Similarly, ground deposits of ash are visible south of the 5 May plume, and are presumed to result from the 3–4 May plume. The edges of these deposits, where visible, are shown on the map in Figure 1a. On 6 May the eruption entered a more intense but short-lived phase, with column height estimates of up to 30 km, producing a cloud that drifted NE across the Andes, before spreading eastward, and then ENE across Argentina. A second burst later in the day resulted in similar plume trajectories, and ash fallout the following day occurred as far as 1000 km from source [*Folch et al.*, 2008]. A further explosive phase, of unknown intensity, occurred on 8 May, with transport directions corresponding closely to those of the 6 May. Extensive ash deposits from the 6–8 May episodes are visible on the 12 May MODIS image, as far as the Atlantic coast of Argentina. Explosive activity continued,

[1] Department of Earth Sciences, University of Oxford, Oxford, UK.
[2] Department of Earth Sciences, University of Cambridge, Cambridge, UK.

0148-0227/09/2008JB006219$09.00

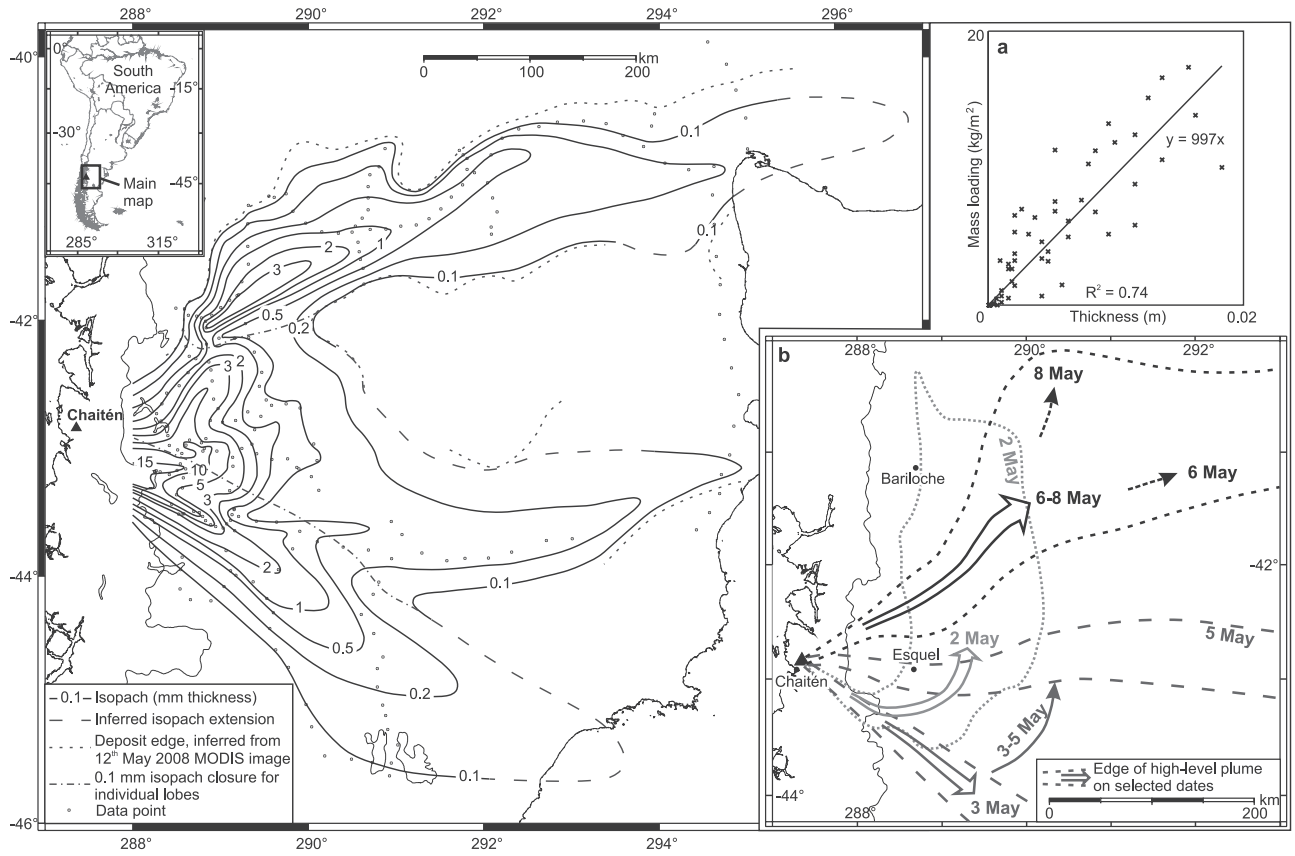

Figure 1. Isopach map of the Chaitén distal ash deposit. Isopachs are drawn by hand and extended to the approximate Andean watershed (288°longitude). Individual ashfalls are identifiable distally, for example, from 3 (southernmost) and 6 May (northernmost), but in the Argentinean border regions units overlap, with an additive thickness effect. Deposit edges, inferred where possible from satellite images, correspond with and fall slightly outside the mapped 0.1 mm isopach. (a) Ashfall mass loading against thickness. The linear relationship allows an estimation of deposit density at 997 kg m^{-3}. (b) Plume dispersal over Argentina during the first week of eruption, mapped from MODIS images. Ash deposition corresponds accordingly, with some modification by low-level local winds.

but with much lower plume heights in the range of 2–5 km, throughout the following months. There is little evidence that this subsequent activity resulted in measurable fallout in Argentina, except for minor ashfall observed in the border regions on 30–31 May, and the volume of distal ash fallout in Argentina from this continuing activity is considered negligible in comparison to the 2–8 May period.

2. Ash Sampling

[4] Fieldwork was conducted across affected regions of Argentina from 30 May to 11 June 2008, using MODIS images showing plume dispersal to guide sampling. Ash samples, and thickness and mass-loading measurements, were taken at 227 sites transecting the deposit (Figure 1; Figures S1 and S2 in the auxiliary material).[1] Heavy rainfall in mid-May had disturbed the deposit in places. In such locations, measurements were taken in protected spots, or by taking an average thickness across the site. At higher elevations snowfall disturbed the deposit to a lesser extent. The ash formed a continuous surface crust at thicknesses >0.5 mm; below this, wind erosion resulted in patchy preservation. There was clear evidence in most areas of the influence of rain and wind erosion on the deposit, particularly where the deposit was thinnest, and preservation here was restricted to sheltered pockets, such as pits in rock or pieces of refuse. Care was taken at such sites to take measurements and samples from such locations. In some cases a degree of accumulation had occurred in these sheltered spots owing to rain washing. In such locations, an average site measurement was produced by estimating the area of washing in (in as many places as possible). Thus, while the deposit was no longer pristine in many areas, because the removal or reworking of ash by wind and water action had not been wholesale, and by carefully selecting sampling sites, we were still able to take measurements. It remains possible that some degree of winnowing of fines occurred, though the degree to which this may have taken place remains unclear. Using these methods, we were able to map self-consistently to low ash thicknesses, adopting as a minimum criterion [cf. *Martin-Del Pozzo et al.*, 2008] an assigned thickness of <0.1 mm where ash was detectable only as a pale dusting on stiff leaves. Both local people's estimates of fresh ashfall thickness, and that

[1]Auxiliary materials are available in the HTML. doi:10.1029/2008JB006219.

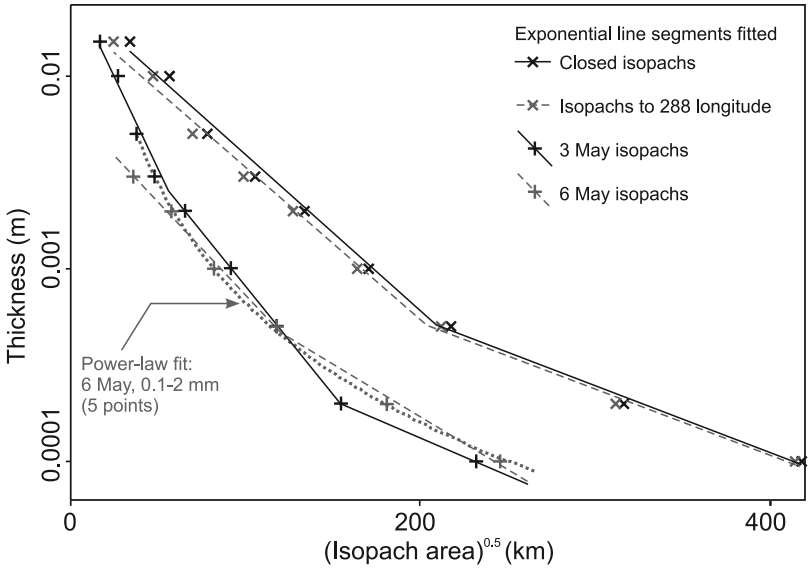

Figure 2. Isopach area against thickness, with straight-line (exponential) segments fitted and a power law fit for the 6 May deposit. Areas for the whole deposit were found by closing mapped isopachs around the volcano location, while extrapolation of distal isopachs distinguished the 3 and 6 May deposits such that the 6 May deposit centers around a secondary maximum and the 3 May closes around the volcano. More rapid proximal thickening (a steeper line segment) is likely in each case and necessary to prevent the 3 May segment, when extrapolated back, from projecting above the whole deposit data.

estimated from coupled meteorological and dispersal models [*Folch et al.*, 2008], correspond well with our data. In some cases a discrepancy exists, with our measurements being slightly lower than fresh thickness estimates. This is likely to be a result of closer particle packing and settling of the deposit upon wetting by rainfall, resulting in a thinner, but denser deposit, when compared to the fresh ashfall.

3. Results and Discussion

3.1. Ash Distribution

[5] Ash thicknesses, plotted on isopach maps (Figure 1), reveal a complex distribution corresponding closely to plume transport directions during different phases of the eruption. Deposit edges inferred from MODIS satellite images lay slightly outside the 0.1 mm isopach, validating our interpretation that thin, fresh ashfall is observable remotely. This correspondence of our mapped ash distribution with the edges of fresh ashfall observed on MODIS images indicates that wind-driven remobilization and redeposition of ash had not occurred over spatial scales large enough to alter the primary distribution. When mapped, our measured thickness values show a highly self-consistent pattern, predominantly decaying with distance. This suggests that, in spite of reworking and removal of ash in many locations, our approach of selecting sheltered localities and taking site averages of thickness was valid. A more erratic pattern would be expected if removal, redeposition and accumulation had affected our measurements to a significant degree.

[6] Individual eruption phases produced discrete ash units, which overlap in a complex fashion in medial regions (<200 km from the vent). In more distal locations (>200 km from the vent), ash fallout from discrete eruptive phases may be distinguished when transported over areas without previous ashfall (e.g., 3 and 6 May; Figure 1), and is the result of multiple eruption phases over a time period sufficient to encompass changes in wind conditions. The total area enclosed by the 0.1 mm isopach is $\sim 1.7 \times 10^5$ km^2, much larger than that of the Fuego 1974 deposit ($\sim 3 \times 10^3$ km^2) [*Rose et al.*, 2008], but comparable to the 1980 Mt St Helens eruption ($\sim 3 \times 10^5$ km^2) [*Bonadonna and Houghton*, 2005]. The 1 mm isopach area (2.9×10^4 km^2) suggests that the Chaitén eruption was an order of magnitude smaller than that of Hudson, 1991 (1.1×10^5 km^2) [*Scasso et al.*, 1994]. However, such thickness-based comparisons should be treated with a degree of caution, since our measured thicknesses potentially reflect a degree of postdepositional compaction, and may not be directly comparable to fresh measurements made for other fall deposits. Thus, such comparisons may slightly underestimate the scale of the Chaitén eruption. The bulk deposit density at the time of sampling, estimated from sites where weighed samples were collected over measured areas (Figure 1), indicates a mean of 997 kg m^{-3}, and is within the range expected for a rhyolitic ashfall deposit. The fresh deposit (i.e., prior to rainfall) is likely to have had a slightly lower bulk density than the deposit measured in the field. If the only postdepositional change to the deposit is an increase in bulk density, then this does not affect our mass or dense rock equivalent volume estimates. Therefore, quoting eruption size in terms of mass, and deposition in terms of mass loading, is more meaningful, and more readily transferable for the purpose of interevent comparisons, than magnitudes based on tephra thickness or volume alone.

3.2. Eruption Volumes

[7] Using plots of the logarithm of ash thickness, T, against the square root of isopach area, A (Figure 2) we determine ashfall volumes by integration [*Pyle*, 1989, 1995; *Fierstein*

Table 1. Estimates of Eruption Volumes and Magnitude

	Whole Deposit With Isopachs Closed[a]	Whole Mapped Deposit[b]	3 May Lobe[c]	6 May Lobe[d]
Volume[e] (km^3)				
Exponential	0.17	0.15	0.05	0.03
Power law	-	-	-	0.04
Magnitude [*Pyle*, 2000]	4.24	4.19	3.69	3.54
Volume inside 0.1 mm isopach[e]	0.16	0.14	-	0.03
Total grain size mode(s) (μm)	-	-	46	30;115
Total grain size 98th percentile (μm)	-	-	320	435

[a]These estimates are minimum values. An increased rate of proximal thickening is likely, and, for example, a maximum deposit thickness of 1 m would increase the volume to 0.24 km^3 and the magnitude to 4.37.
[b]Western limit of isopach mapping at 288° longitude.
[c]Isopachs closed around volcano.
[d]Estimates based on deposit centered around the secondary maximum in Argentina, thus not directly comparable to data calculated for isopach closure around the volcano.
[e]Volumes, in km^3, can be converted to mass, in kg, by multiplying these values by 10^{12}.

and Nathenson, 1992]. On such plots, straight-line segments are defined by exponential decay, describing an exponential cone

$$T = T_0 \exp\left(-kA^{0.5}\right)$$

where k is the line slope and T_0 is the maximum deposit thickness. Integrating below the cone to find V gives

$$V = 2\left(T_0/k^2\right)$$

To account for multiple straight-line segments, resulting from increasingly rapidly decaying proximal deposit thicknesses, we apply a correction, p, to each of N segments, deriving [from *Pyle*, 1995]

$$p_N = \left(2/k_{n+1}^2\right)\{T_{n+1} - T_x[1 - \ln(T_x/T_{n+1})]\} - \left(2/k_n^2\right) \times \{T_n - T_x[1 - \ln(T_x/T_n)]\}$$

where n and n+1 represent values obtained from the line segment at distances larger and smaller than the break in slope, respectively, and T_x is the deposit thickness at the break in slope. Thus, using T_0 and k from the most distal straight-line segment, total deposit volume is

$$V = 2\left(T_0/k^2\right) + p_1 + \ldots + p_N$$

From *Fierstein and Nathenson* [1992] the volume inside a particular isopach, of area A is found using

$$V = \left(2T_0/k^2\right)[1 - (kA + 1)\exp(-kA)]$$

and a correction, p, must again be applied where necessary.

[8] All our isopach data can be approximated by two or three exponential segments, as commonly observed for explosive eruption deposits (Figure 2) [*Pyle*, 1989; *Bonadonna and Houghton*, 2005]. From this we estimate that 1.6×10^{11} kg of ash was deposited over Argentina. This is equivalent to a tephra volume of 0.16 km^3, or a dense rock equivalent volume of 0.07 km^3, assuming a density of 2.35 kg m^{-3} for crystal-poor rhyolite. Similarly, we estimate a minimum total tephra volume of 0.17 km^3 (Table 1), a mass of 1.7×10^{11} kg. This estimate projects the thickening rate derived from our mapped regions to the volcano location, and in reality, based on observations elsewhere [*Pyle*, 1989; *Bonadonna and Houghton*, 2005], more rapid proximal thickening is likely. For example, assuming proximal thickening to a maximum of 1 m, based on events of similar magnitude, we produce a total tephra mass of 2.4×10^{11} kg, using the same density for the proximal deposit as for the distal. Although the proximal thickening rate is unconstrained, this estimation demonstrates the potential uncertainty in eruption volumes produced using only distal data. We estimate that ~70% of ash, by volume, produced by the eruption fell east of 288° longitude, over Argentina and the Atlantic Ocean.

[9] The 6 and 8 May eruptive phase, as described in the introduction, involved up to three short-lived energetic explosions, with similar plume transport directions. The relative intensity of these episodes is unclear, but the 8 May cloud may have drifted northward in mid-Argentina (Figure 1b) [*Folch et al.*, 2008] rather than following the easterly direction of the 6 May. For simplicity, we refer to this northern depositional lobe as the 6 May deposit. This produced a 0.1 mm isopach extending up to ~800 km from the volcano, and accounts for 22% by volume of the mapped Argentinean ashfall, forming closed isopachs around an isolated maximum ~200 km NE of Chaitén. This unit, midgray in color, was distinctively coarser in mid-Argentina than the paler deposit resulting from earlier eruption phases, and thinned toward the Andean region. Given these field observations and our mapped isopach dispersion patterns it is likely that the isolated isopachs represent a secondary thickness maximum, rather than arising simply from overlap with the 2 May fallout, although this may have added complexity to the distribution. If this is the case, more proximal thickening is likely to occur in the unmapped region toward the volcano. Such a feature may arise from fine-particle aggregation [*Carey and Sigurdsson*, 1982; *Brazier et al.*, 1983], resulting in a larger effective grain size, owing to ash interaction with frozen or liquid hydrometeors [*Textor et al.*, 2006; *Durant et al.*, 2008]. The less explosive 3 May eruptive phase produced 0.05 km^3 of tephra, dispersed by strong winds (Figure 1), and depositing ash in a sharp-edged linear lobe. The complex distribution of the 2 May deposit, affected by later ash overlap (Figure 1), does not permit its volume to be estimated.

[10] We estimate that <8% of the whole deposit volume lies beyond the 0.1 mm isopach, increasing to 14% for the 6 May unit. This may reflect a higher 6 May eruption column,

but is potentially an artifact of deposit overlap elsewhere, thickening distal ashfall through repeated or long-lasting deposition. These estimates are made on the basis of extrapolating the most distal exponential segment. It is not clear whether thickness decay remains exponential at distances beyond a few hundred km, and more gradual decay may occur, since the grain size distribution may change very little with distance, with meteorological factors potentially having a significant effect on particle sedimentation.

[11] A multiple-segment exponential decay model fits our data for the whole deposit well (Figure 2), and has a sound physical basis, with a maximum thickness decaying to zero. However, individual units are not described by a single exponential segment, perhaps reflecting depositional complexities, whereby multiple phases occur within an apparent single mappable unit, or changing controls on particle settling and diffusion with distance, grain size and Reynolds number [*Ernst et al.*, 1996; *Bonadonna et al.*, 1998].

[12] For tephra deposits with few distal data points the extrapolation of a proximal exponential segment can produce volume underestimation [*Bonadonna and Houghton*, 2005], and a power law relationship may better represent the deposit:

$$T = T_{\mathrm{PL}} A^{-m/2}$$

Here, T_{PL} is a constant and m is the power law coefficient. Deposit volume is found using

$$V = (2T_{\mathrm{PL}}/(2-m))\left(C^{2-m} - B^{2-m}\right)$$

where B is defined by the maximum thickness predicted from the exponential relationship, such that $B = (T_0/T_{\mathrm{PL}})^{-1/m}$ and C is the downwind distance limit of volcanic cloud spreading, assessed from satellite images [*Bonadonna and Houghton*, 2005].

[13] As expected from its temporal and spatial complexity, a single power law does not fit the whole Chaitén deposit. However, a power law curve fits the 6 May unit (Figure 2, the inner point misfit may be attributed to our lack of proximal data). Estimating downwind plume dispersion, C, of 800 km, we produce a volume 19% larger than that found using exponential segments. Again, it is unclear whether a single power law would be expected to hold at the most distal locations, where factors influencing fallout are likely to change. Problems also arise in this method through the subjective selection of integration limits, particularly C, and we suggest the exponential segment method to be most appropriate in this case, providing a good fit to the data and requiring the fewest assumptions. Our estimated volumes and bulk ash density of 997 kg m^{-3} indicate a minimum deposit mass of 1.7×10^{11} kg, or an eruption magnitude, (defined as magnitude = $\log_{10}$(erupted mass, kg) − 7) [*Pyle*, 2000] of >4.2 (Table 1), suggesting that Chaitén was the largest explosive eruption globally since Hudson, 1991.

3.3. Deposit Grain Size

[14] Grain size was measured for 140 samples by laser diffraction size analysis, using a Malvern Mastersizer 2000 with Hydro MU attachment, with a refractive index of 1.52 and absorption coefficient of 0.1. Replicate samples from 13 sites showed good reproducibility of distribution shape and modes. Samples contaminated by dirt, recognizable from anomalous coarse modes, or with skewed size distributions resulting from postdepositional erosion were rejected. Several samples showed bimodality, and very few showed a smooth lognormal shape, with many unimodal curves being skewed or showing a shoulder on one or both limbs, potentially indicating multiple populations within a single grain size distribution.

[15] Winnowing of fine material, by either wind or water erosion, may have affected the grain size distributions of samples, even if such processes did not clearly alter our thickness measurements, since any removal of material is likely to be selective toward the finest particles. One feature of our data, which suggests the collected samples were representative of the original material, lies in the consistency seen in distribution shape over large areas, such as those for all samples of the 3 May depositional lobe (Figure 3). In contrast, degrees of winnowing would be expected to vary locally, depending on the particular environment from which a sample had been collected, leading to differences in distribution shape between sites. In a few cases, predominantly from the most distal locations, where sample collection had been most difficult, such secondary alteration was immediately apparent from anomalous grain size distribution shapes, and these outliers were removed from our analyses. Otherwise, however, winnowing processes do not appear to have altered our samples significantly. Further evidence in support of this arises from sites in the Esquel region, revisited in January 2009, seven months after our original fieldwork. Thicknesses had changed relatively little during this time period, and by an approximately constant amount (i.e., similar absolute reductions in thickness). As such, deposits originally measured at 3 mm thickness or more remained largely intact as a continuous cover, with reductions of the order of 2 mm, but still forming a surface crust. Thicker deposits, such as those near the Chilean border, originally measured at 10–15 mm, had thus only decreased by a relatively small proportion (<20%). Originally thinner deposits had mostly disappeared as a surface cover, with evidence remaining in sheltered localities, such as around the base of large stones. For deposits originally measured at 1.5 mm or below, virtually all evidence of the ashfall had disappeared. In short, the ashfall remained surprisingly persistent, in spite of its extremely fine-grained nature, wherever the original deposit thickness had exceeded a few mm. Unexpectedly, this may have been aided by rainfall, since the deposit commonly formed a cohesive surface crust, presumably on drying, offering a degree of resistance to erosion, and the early wetting of the deposit may in fact have helped its short-term preservation. In some areas, low-level ground plants had stabilized the deposit and incorporation within the soil sequence had begun to occur. In spite of the semiarid, frequently windy conditions of the region, we suggest that ground vegetation and surface crusting helped stabilize the deposit, and at thicknesses above a few mm, the ashfall was not as ephemeral as might initially be thought. Grain size measurements from the January 2009 samples also confirm that winnowing had not occurred to a significant degree in the 7-month period since initial sample collection (Figure 4). Samples collected from sheltered localities, showing a lack of internal structure, with a locally representative thickness and, in some cases, with surface crusting were deemed to be in

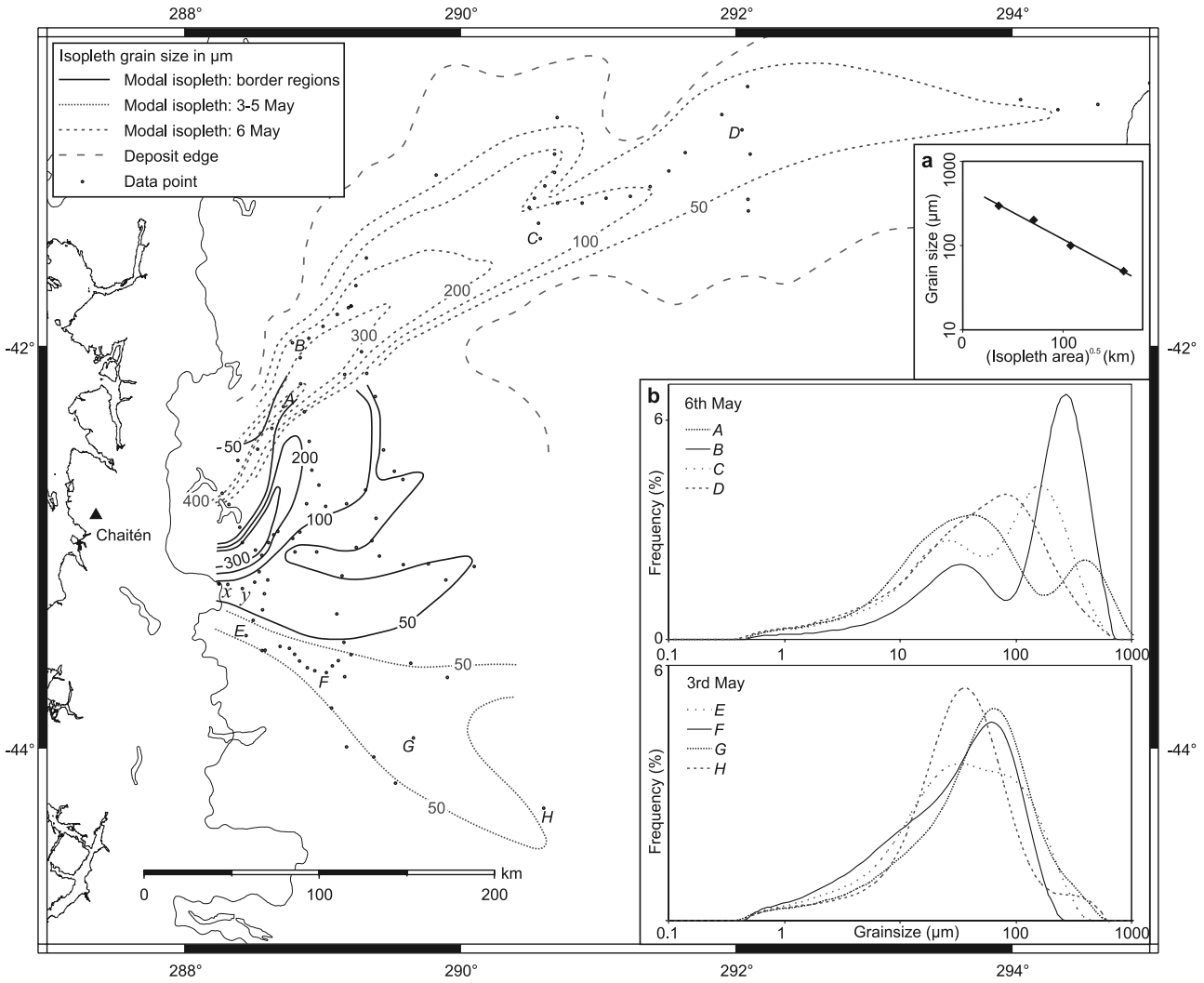

Figure 3. Isopleth map and grain size distributions. Isopleths drawn for modal grain size, with samples marked as black dots. For bimodal distributions the coarser mode is used. Isopleths are distinguished for the 3–5 and 6 May deposits and for the remainder, resulting from complex deposit overlap but dominated by the 2 May fallout, which, with the 6 May, is far coarser than intervening ashfalls. (a) Plot of $(\text{area})^{0.5}$ against ln(grain size) for the 6 May isopleths, showing an exponential decay in coarse mode grain size. (b) Selected grain size distributions for the 3 and 6 May fallouts. Locations marked on main map. The bimodality and distance-related decay for the 6 May contrasts with the relatively stable unimodal character of 3 May. Curve E shows bimodality due to overlap with finer deposits in the border region, while curve H may suffer from both coarse contamination and fine-particle removal through wind erosion, a problem encountered in thinner distal deposits. Locations marked "x" and "y" refer to Figure 4.

their original position. These showed no changes in grain size distribution (Figure 4). In contrast, where ash was accumulated by runoff (commonly showing fine-scale laminations) the grain size distribution was narrowed, with a loss of fines (Figure 4). The main process of deposit alteration in the region (which had already occurred to some extent by the time of initial fieldwork) was through water runoff accompanied by a loss of fines. Deposits affected by this process were highly localized, commonly occurring around the edges of impermeable surfaces such as paved roads. Such locations were easily recognizable and could be avoided during sample collection.

[16] Modal grain size, a precisely measurable parameter, generally unaffected by coarse particle contamination, was used to construct isopleth maps. For multimodal distributions, the coarsest mode was selected. The various units distinguished (Figure 3) correspond well with mapped isopachs (Figure 1). The 6 May modal grain size trend shows exponential decay with a single line segment. However, without sufficient data from other units, this cannot be confirmed as a general case. West of the 6 May thickness maximum, grain size increases as thickness decreases. In some of these medial areas the 6 May modal grain size exceeded thickness, and the deposit was visible as scattered white pumices up to ~1 mm in diameter, lying on earlier ashfall. The ubiquity of this feature in these localities, and the strong bimodality of grain size distributions in this region, with a prominent fine mode, indicates that this does not result

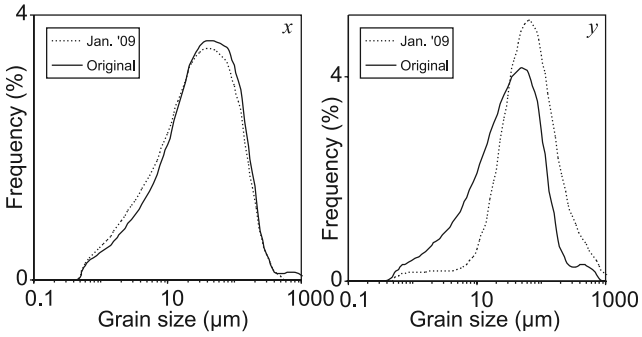

Figure 4. Grain size distributions from two locations near the Chilean border (x and y in Figure 3), where thicknesses exceeded 1 cm. At each site sampling was conducted initially on 5 June 2008 and subsequently on 11 January 2009. At site x the 2009 sample was taken 1 km east of the original location, from a deposit that appeared undisturbed. The grain size distribution is unaltered from the 2008 condition. At site y the 2009 sample was taken at the same location, from a water-accumulated, stratified deposit. The 2009 sample shows the effects of grain size distribution alteration: A long, flat, fine tail; a narrowed peak; and possibly, in this instance, coarse-particle contamination.

from winnowing of fine material. This demonstrates that the overlap of deposits from different eruption phases is one mechanism characteristic of the Chaitén deposits that leads to multiple populations within a single grain size distribution.

[17] The 6 May unit shows grain size bimodality, with modes at a stable ~25 μm and at a coarser value, which decreases steadily with distance from ~300 μm, such that the modes merge in a unimodal distribution ~400 km from the volcano (Figure 3). There are several possible explanations for this complexity in grain size distribution shape. One is that, in addition to the buoyant column, a coignimbrite cloud may have been present during individual eruption phases. This could give rise to tephra populations of different granulometries, in clouds at different heights. However, such an explanation is not necessary to explain the complex tephra dispersal pattern, since this is well accounted for by the changing wind conditions during several days of eruption. Furthermore, there is not at present clear evidence from the region around Chaitén for the occurrence of large-scale pyroclastic flows sufficient to generate coignimbrite clouds of sufficient size to produce this feature. We therefore suggest that the grain size distribution complexities arise both from multiple deposit overlap and from fine-particle aggregation processes. For example, the 6 May deposit overlaps with those from earlier days in the medial region north of Esquel (Figure 1), and here some of the complexity of shape is due to this overlap. In addition, the unit itself is the product of two or three similar explosive pulses, potentially introducing further overlap-type complexities. We suggest that the finest mode seen in the 6 May deposit reflects a different process, of fine-particle aggregation. Both the stability of this peak with distance, remaining static at ~25 μm, and its fineness (e.g., when compared to the 3 May deposit at similar distances) points to the possibility that aggregation led to volumetrically large proportions of fines falling out relatively early. Grain size data identified from the 2 May deposit show similar features. In contrast, ashfalls from the 3–5 May are finer and unimodal, fining only gradually with distance, with a highly consistent distribution shape and a mode, at ~60 μm, coarser than the fine mode of the bimodal units. This suggests a sustained activity level from 3 to 5 May, with a lower column height than the more intense 2 and 6 May phases. Cloud height differences may explain the lack of a clear aggregation-type signature in the 3–5 May deposits, if higher eruption clouds result in more efficient fine-particle aggregation and scavenging through frozen hydrometeor interactions [e.g., *Durant et al.*, 2008].

[18] Total grain size distributions (Figure 5) for the tephra deposited over Argentina, were estimated for the 3 May (15–

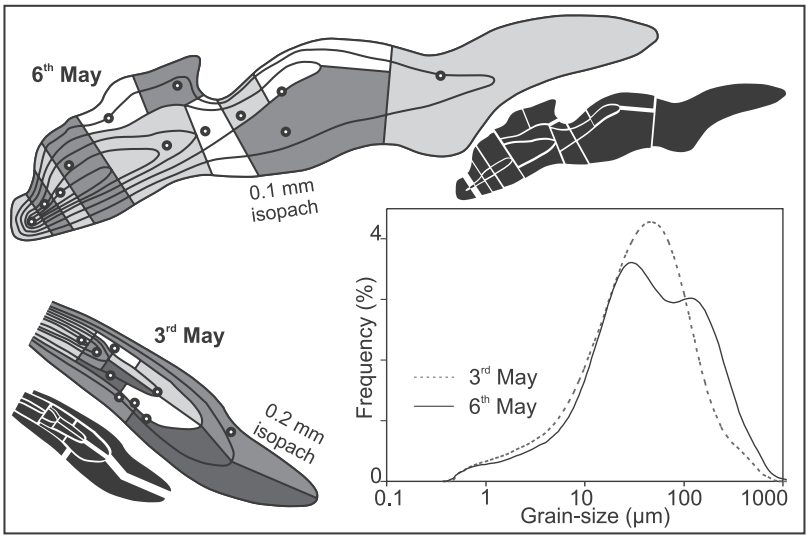

Figure 5. Shaded maps, showing isopachs for the 3 and 6 May deposits (Figure 1), divided into sectors around selected points (black ringed circles) and used to estimate total distal deposit grain size. Further sector subdivisions, by isopachs, are shown in the silhouettes. These areas were used to weight each selected grain size distribution using an assigned thickness of the geometric mean of enclosing isopachs. The distributions thus estimated are shown in the graph.

2 mm isopach range) and 6 May (down to 0.1 mm thickness) units by dividing the deposit into sectors around selected sites, a modification of the method of *Carey and Sigurdsson* [1982]. Given the wide coverage but relatively sparse distribution of our data points, we selected this method over alternatives [e.g., *Bonadonna and Houghton*, 2005]. Sectors were separated perpendicular to the deposit axis, where possible at the midpoint of successive sites or at the nearest mapped isopach. Sectors were split on the basis of isopachs, and each subdivision received a representative thickness from the geometric mean of the enclosing isopachs. The product of subdivision area and thickness gave a weight to the grain size distribution of a particular sector, the sum of which provided a total grain size distribution estimate. The data confirm a finer 3 May deposit, and show bimodality in the 6 May fallout (Table 1).

[19] With respect to respiratory hazard [*Horwell and Baxter*, 2006], both deposits have similar total proportions of thoracic (<10 μm) material. For the 6 May this increases from 10% in the border regions to 20% distally, and is generally 20–25% for other units, approaching 30% distally. The respirable (<4 μm) proportion varies similarly, ranging from 5% in medial regions of the 6 May unit to 15% in other distal areas, a similar proportion to that in Mt St Helens' 1980 ash at comparable distances [*Durant*, 2007]. However, importantly for health concerns, locally resuspended ash is likely to contain a greater proportion of fine material than that estimated for the whole deposit (R. S. Martin et al., Environmental effects of ashfall in Argentina from the 2008 Chaitén volcanic eruption, submitted to *J. Volcanol. Geotherm. Res.*, 2009).

3.4. Ash Chemistry and Potential Impacts

[20] Bulk ash compositional analyses, undertaken on four ash samples by X-ray fluorescence spectroscopy, and glass analyses on 219 points of fifteen ash samples by electron microprobe (Table 2), have been combined with compositional data on the recent and previous eruptions of Chaitén [*Naranjo and Stern*, 2004; *Horwell et al.*, 2008]. With calculated CIPW norm compositions [*Kelsey*, 1965] and examination of particles by scanning electron microscope, this shows the eruption involved a weakly peraluminous rhyolitic melt, lacking phenocrysts, with minor proportions of plagioclase and rarer biotite microlites, and a mean glass silica content of 74.5 wt % (Figure 6). Distal ash lacked lithic and crystal components, comprising variably vesicular pumice and glass shards. Ash composition was relatively uniform, with subtle chemical differences between eruptive phases suggested by discrete domains within the overall compositional range occupied by samples from specific depositional lobes (Figure 6b). The ash has similar silica content to, but is more sodic and less potassic than, the ~10 ka Chaitén (Cha1) ash [*López-Escobar et al.*, 1993; *Naranjo and Stern*, 2004]. Rhyolites are rare in this portion of the southern Andean volcanic arc, the only regional tephra of comparable composition being the eastward dispersed Mic2 unit (Figure 6), identified as originating from Minchinmávida, 20 km east of Chaitén [*Naranjo and Stern*, 2004]. However, this rock composition is not typical of that produced by Minchinmávida, and the identification of the source volcano, based on a lack of the Mic2 tephra outcropping west of Minchinmávida, may not be correct, with Chaitén as the alternative. Field mapping of the Cha1 and Mic2 tephra [*Naranjo and Stern*, 2004; S. Watt et al., unpublished data, 2009] suggest that, in comparison with the current Chaitén eruption, although compositionally similar, these events were significantly larger in magnitude. The only other documented regional rhyolite is a sample from Yate [*Mella*, 2008], 140 km to the north, though again this is atypical of the volcano. Thus, the rhyolite produced at Chaitén is unusual in a regional context, yet is the only magma type produced in significant volumes during the known activity of Chaitén. The homogeneous compositional character of the current eruptive episode does not provide evidence for the involvement of mafic magma in the eruption, and the highly evolved nature may be a result of long-term magma storage and melting of the granitoid basement, resulting in infrequent eruptions of highly evolved magma. It remains unclear, however, why this situation is not encountered at other regional centers. The Hudson 1991 ash [*Gutiérrez et al.*, 2005; *Kratzmann et al.*, 2009], the product of the only other historic large explosive eruption in the region, is far less evolved, with a broader compositional range.

[21] Comparison of incompatible trace element concentrations in the Chaitén ash with other southern Andean volcanoes suggests distinct evolutionary paths for the Chaitén magma (Figure 6). While the Rb data suggest a trend potentially consistent with fractionation of a melt similar to those erupted at Hudson, Zr shows significant differences, and the compositions are distinct from the fractionation trend defined by volcanoes located between Chaitén and Hudson [cf. *Naranjo and Stern*, 1998]. These data again show a close similarity between the Mic2 tephra and Chaitén's volcanic products, while other Minchinmávida volcanics do not correspond with Mic2. The trace element data are consistent with a model whereby significant crustal assimilation occurred in the Chaitén magma, through wholesale melting of Patagonian batholith granitoids, and major element data [*Pankhurst et al.*, 1999] are also consistent with such a process.

[22] Following the method of *Blundy and Cashman* [2001], compositional norms of glass and bulk ash, plotted on the granitic ternary diagram (Figure 6), are consistent with magma equilibration under water-saturated conditions at ~100–200 MPa, or ~3–6 km depth, where dissolved water content of up to 6 wt % [*Tamic et al.*, 2001] may explain the high eruption explosivity. Earthquakes recorded beneath Chaitén in 2005 at ~10 km depth [*Lange et al.*, 2008] may thus correspond to deeper magma chamber replenishment, precursory to the eruption.

[23] From the volumes lying beyond our mapped isopachs, we estimate that 5% of the ash (9×10^9 kg) fell over the Atlantic Ocean, mostly of grain size <50 μm. Eruptions of this magnitude are potentially recorded in Argentine shelf sediments, and are periodic contributors to the Antarctic and Southern Ocean dust budget [*McConnell et al.*, 2007]. Comparison with Patagonian dust (Figure 6), for which Andean volcanic ash of the more common andesitic composition forms an important component [*Gaiero et al.*, 2007], shows that rarer rhyolitic ash, such as that from Chaitén, is a minor dust component. The low iron content of Chaitén glass (<1 wt % FeO) suggests this ash would have had a minor impact on nutrient-limited portions of the Southern Ocean

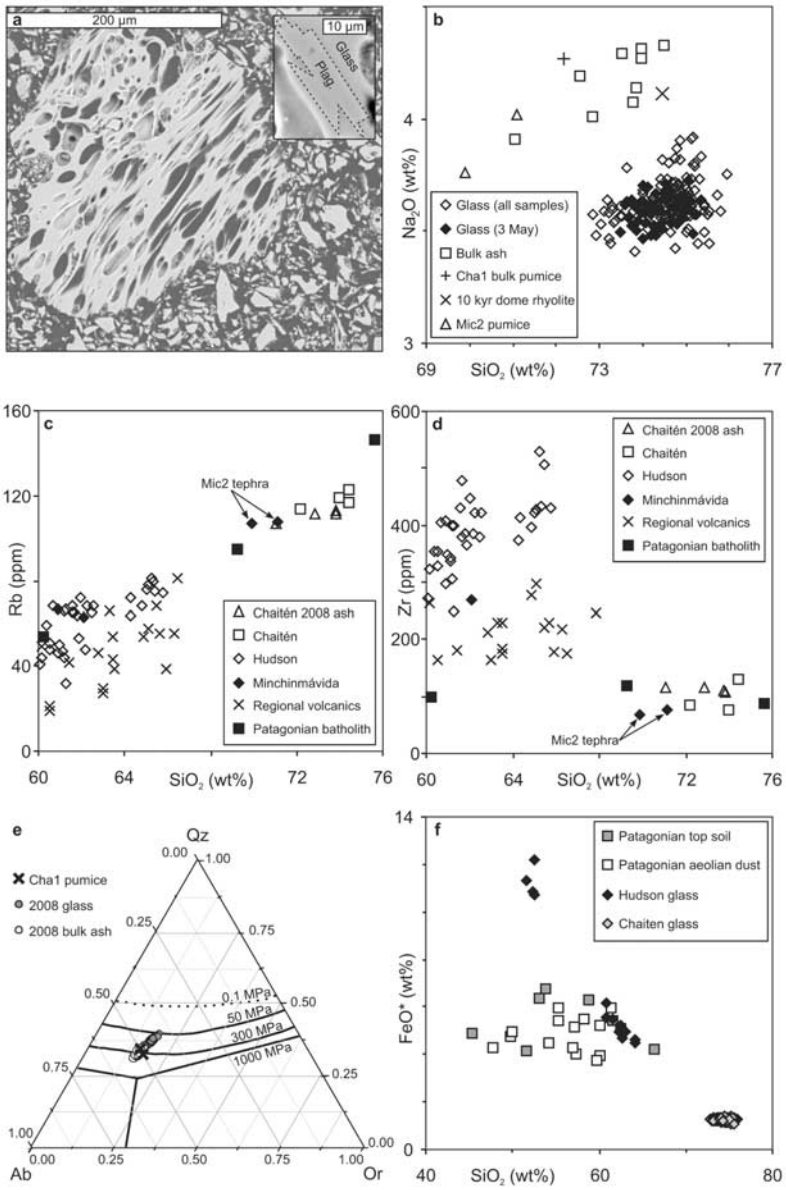

Figure 6. (a) Scanning electron microscope image of highly vesicular pumice from the 2 or 6 May ashfall, collected 150 km from the volcano. Inset shows plagioclase microlite (outlined; 71 mol % Albite) within the same sample. (b) Na_2O against silica content for glass and bulk ash (our data, *Horwell et al.* [2008], and *Naranjo and Stern* [2004]) from the recent Chaitén eruption and that at ~10 ka (Cha1), with a rhyolitic pumice from nearby Minchinmávida volcano (Mic2) shown for comparison. The glass forms a single compositional group, but the 3 May data cover a discrete domain within this, suggesting slight compositional differences between eruption phases. (c–d) Rb and Zr against silica for regional volcanics containing >60 wt % SiO_2 [*D'Orazio et al.*, 2003; *Gutiérrez et al.*, 2005; *Kilian and López-Escobar*, 1991; *López-Escobar et al.*, 1993; *Naranjo and Stern*, 2004; *Notsu et al.*, 1987]. Points are shown for bulk tephra or lava from Hudson, occupying a distinct group [cf. *Naranjo and Stern*, 1998], and for volcanoes between Hudson and Chaitén (Cay, Corcovado, Maca, Melimoyu, Mentolat, and Yanteles), as well as for Chaitén, distinguishing our data of the 2008 ash from those relating to older Chaitén volcanics [*Kilian and López-Escobar*, 1991; *López-Escobar et al.*, 1993; *Naranjo and Stern*, 2004]. Data are also given for local samples of the Patagonian Batholith (from Futaleufú and Palena) [*Pankhurst et al.*, 1999]. Data from Minchinmávida are shown separately, with the Mic2 tephra labeled. (e) Glass compositions of glass and bulk ash plotted on the granitic ternary diagram (method from *Blundy and Cashman* [2001]) and compared with the Cha1 tephra [*Naranjo and Stern*, 2004]. The glass composition suggests equilibration at pressures corresponding to magma chamber depths of ~3–6 km. (f) FeO* (assuming all Fe present as FeO) against silica for the Chaitén 2008 glass and glasses from the compositionally mixed Hudson 1991 eruption [*Kratzmann et al.*, 2009] compared to the compositions of modern Patagonian topsoils and aeolian dust [*Gaiero et al.*, 2007].

Table 2. Bulk Ash and Glass Compositions of Chaitén Ash[a]

	Bulk Ash[b]				Chaitén Glass[c]					
	0507a	0512a	0520a	0616b	0518B/14	3008/11	0408/8	0608/3	0707/13	Average (219 points)
Longitude	−43.173	−43.432	−43.594	−42.056	−43.528	−42.683	−43.155	−42.723	−42.509	-
Latitude	−71.751	−71.557	−71.112	−71.163	−71.204	−71.028	−70.107	−71.729	−70.559	-
Distance to Chaitén (km)	82	111	151	149	140	133	210	76	175	-
Ash thickness (mm)	18	9	6	3	10	3	0.5	1	0.4	-
Modal grain sizes[d] (μm)	30;95	32;78	67	314;42	67	32	59	61;400	21	-
Major elements (wt %)										
SiO_2	73.78	71.06	72.85	73.86	74.49	75.05	74.44	75.01	74.04	74.50
TiO_2	0.150	0.246	0.195	0.162	0.16	0.14	0.14	0.14	0.13	0.14
Al_2O_3	13.76	14.17	13.83	13.96	13.87	13.53	13.91	14.00	13.82	13.86
Fe_2O_3	1.51	2.23	1.79	1.59	-	-	-	-	-	-
FeO*[e]	-	-	-	-	1.26	1.16	1.28	1.28	1.23	1.27
MnO	0.057	0.065	0.059	0.059	0.00	0.08	0.06	0.06	0.06	0.05
MgO	0.26	0.47	0.33	0.32	0.26	0.18	0.26	0.26	0.24	0.26
CaO	1.47	1.71	1.55	1.62	1.36	1.24	1.39	1.39	1.39	1.35
Na_2O	4.08	3.91	4.01	4.14	3.64	3.51	3.73	3.69	3.60	3.61
K_2O	2.93	2.71	2.86	2.94	3.01	3.08	3.00	3.06	3.09	3.03
P_2O_5	0.062	0.089	0.070	0.068	-	-	-	-	-	-
L.O.I.	0.89	2.38	1.08	1.04	-	-	-	-	-	-
Total	98.95	99.03	98.62	99.75	98.05	97.98	98.21	98.88	97.61	98.07
Trace elements (ppm)										
Rb	113	107	111	111	-	-	-	-	-	-
Sr	145	161	152	153	-	-	-	-	-	-
Y	13.4	16.8	14.4	13.7	-	-	-	-	-	-
Zr	109	117	115	109	-	-	-	-	-	-
Nb	7.8	8.1	8.4	7.7	-	-	-	-	-	-
Ba	604	597	599	599	-	-	-	-	-	-
Pb	19	19	21	20	-	-	-	-	-	-
Th	11	12	13	12	-	-	-	-	-	-
V	13	27	12	11	-	-	-	-	-	-
Cu	4	22	13	5	-	-	-	-	-	-
Zn	35	42	39	36	-	-	-	-	-	-
Ga	13	14	14	14	-	-	-	-	-	-
As	15	15	16	17	-	-	-	-	-	-

[a]Glass composition shown for five selected samples, with an average of all analyses.
[b]Measured by XRF at Open University Department of Earth Sciences, Milton Keynes, U.K. Cr, Co, Mo, Ni, S, Sc, U were around or below the detection limit. Results were mostly within 2% of reference values for three standard materials for major elements, and within similar levels for four standards for trace elements, except for Zn and Pb (4%), Cu (6%), and Nb (9%).
[c]Analyses by electron microprobe: beam diameter 10 μm, beam current 15 nA.
[d]Main distribution peak listed first if bimodal.
[e]FeO*, total Fe as FeO.

[cf. *Martin et al.*, 1990] in comparison to large explosive andesitic eruptions.

4. Summary

[24] We have mapped the distal ash deposit from the Chaitén 2008 eruption, and produced the first field-based estimates of eruption volume and magnitude. The complexity of ash dispersal is directly related to a changing wind field during the week-long main eruption period, and it is possible, using this dispersal pattern, to reconstruct both the dominant features of this wind field, and to use it to separate individual eruption units. These units are compositionally highly uniform, but sample grain size distributions can be used to elucidate further the transport and deposition of separate units, with both grain size and modality related to changing column height and eruption intensity.

[25] The multiple ash fallout units, each with distinct dispersal patterns and granulometric characteristics, arise from an eruption duration of sufficient length for regional wind conditions to vary significantly, with the complexity amplified owing to variable eruptive intensity in a multiphase event. Explosive eruptions of comparable duration may result in similar complexity, but past event reconstruction often relies only on the more commonly preserved proximal deposits, fitted with elliptical isopachs (and an implicit assumption of a single eruption phase). Our work highlights the uncertainty in extrapolation using sparse data, since the distal Chaitén ash, all at thicknesses below 2 cm, is volumetrically large and spatially complex, but preservation is likely to be highly variable. Magnitude estimates of past eruptions based on data from poorly preserved deposits may thus be rendered highly inaccurate.

[26] The chemistry of the Chaitén 2008 ash, while unusual in a regional context, is highly similar to previous products of Chaitén. The finest, most distal ash from such eruptions, though a periodic contributor to the Patagonian dust budget, is unlikely to be a significant Southern Ocean nutrient source, being low in iron, and volumetrically small in the long term when compared with the more common, compositionally less-evolved, regional tephra.

[27] **Acknowledgments.** This work was supported by an NERC Urgency grant NE/G001715/1. T.M. thanks the Royal Society for financial support. We are grateful to W.I. Rose and two additional reviewers for helpful comments that improved the manuscript. The authors thank A. J. Durant for advice regarding the manipulation of grain size data and also

thank the municipal administration of Esquel, Gustavo Villarosa, and Alfredo Fierro for facilitating fieldwork.

References

Blundy, J., and K. Cashman (2001), Ascent-driven crystallization of dacite magmas at Mount St Helens, 1980–1986, *Contrib. Mineral. Petrol.*, *140*, 631–650.

Bonadonna, C., and B. F. Houghton (2005), Total grain-size distribution and volume of tephra-fall deposits, *Bull. Volcanol.*, *67*, 441–456, doi:10.1007/s00445-004-0386-2.

Bonadonna, C., G. G. J. Ernst, and R. S. J. Sparks (1998), Thickness variations and volume estimates of tephra fall deposits: The importance of particle Reynolds number, *J. Volcanol. Geotherm. Res.*, *81*, 173–187, doi:10.1016/S0377-0273(98)00007-9.

Brazier, S., R. S. J. Sparks, S. N. Carey, H. Sigurdsson, and J. A. Westgate (1983), Bimodal grain size distribution and secondary thickening in air-fall ash layers, *Nature*, *301*, 115–119, doi:10.1038/301115a0.

Carey, S. N., and H. Sigurdsson (1982), Influence of particle aggregation on deposition of distal tephra from the May 18, 1980, eruption of Mount St Helens volcano, *J. Geophys. Res.*, *87*, 7061–7072, doi:10.1029/JB087iB08p07061.

D'Orazio, M., F. Innocenti, P. Manetti, M. Tamponi, S. Tonarini, O. González-Ferrán, A. Lahsen, and R. Omarini (2003), The Quaternary calc-alkaline volcanism of the Patagonian Andes close to the Chile triple junction: Geochemistry and petrogenesis of volcanic rocks from the Cay and Maca volcanoes (~45°S Chile), *J. South Am. Earth Sci.*, *16*, 219–242, doi:10.1016/S0895-9811(03)00063-4.

Durant, A. J. (2007), On water in volcanic clouds, Ph.D. thesis, 242 pp., Mich. Tech. Univ., Houghton.

Durant, A. J., R. Shaw, W. I. Rose, Y. Mi, and G. G. J. Ernst (2008), Ice nucleation and overseeding of ice in volcanic clouds, *J. Geophys. Res.*, *113*, D09206, doi:10.1029/2007JD009064.

Ernst, G. G. J., M. I. Bursik, S. N. Carey, and R. S. J. Sparks (1996), Sedimentation from turbulent jets and plumes, *J. Geophys. Res.*, *101*, 5575–5589, doi:10.1029/95JB01900.

Fierstein, J., and M. Nathenson (1992), Another look at the calculation of fallout tephra volumes, *Bull. Volcanol.*, *54*, 156–167, doi:10.1007/BF00278005.

Folch, A., O. Jorba, and J. Viramonte (2008), Volcanic ash forecast: Application to the May 2008 Chaitén eruption, *Nat. Hazards Earth Syst. Sci.*, *8*, 927–940.

Gaiero, D. M., F. Brunet, J.-L. Probst, and P. J. Depetris (2007), A uniform isotopic and chemical signature of dust exported from Patagonia: Rock sources and occurrence in southern environments, *Chem. Geol.*, *238*, 107–120, doi:10.1016/j.chemgeo.2006.11.003.

Gutiérrez, F., A. Gioncada, O. González Ferran, A. Lahsen, and R. Mazzuoli (2005), The Hudson volcano and surrounding monogenetic centres (Chilean Patagonia): An example of volcanism associated with ridge–trench collision environment, *J. Volcanol. Geotherm. Res.*, *145*, 207–233, doi:10.1016/j.jvolgeores.2005.01.014.

Horwell, C. J., and P. J. Baxter (2006), The respiratory health hazards of volcanic ash: A review for volcanic risk mitigation, *Bull. Volcanol.*, *69*, 1–24, doi:10.1007/s00445-006-0052-y.

Horwell, C. J., S. Michnowicz, and J. Le Blond (2008), Report on the mineralogical and geochemical characterisation of Chaitén ash for the assessment of respiratory health hazard, report, Durham Univ, Durham, U.K.

Kelsey, C. H. (1965), Calculation of the CIPW norm, *Mineral. Mag.*, *34*, 276–282, doi:10.1180/minmag.1965.034.268.23.

Kilian, R., and L. López-Escobar (1991), Petrology of the southern South Andean volcanic zone (41–46°S) with emphasis on the Michinmáhuida-Chaitén complex (43°S), *Zentralbl. Geol. Palaeontol. Teil 1*, *6*, 1693–1708.

Kratzmann, D. J., S. Carey, R. Scasso, and J. A. Naranjo (2009), Compositional variations and magma mixing in the 1991 eruptions of Hudson volcano, Chile, *Bull. Volcanol.*, *71*, 419–439.

Lange, D., J. Cembrano, A. Rietbrock, C. Haberland, T. Dahm, and K. Bataille (2008), First seismic record for intra-arc strike-slip tectonics along the Liquiñe-Ofqui fault zone at the obliquely convergent plate margin of the southern Andes, *Tectonophysics*, *455*, 14–24, doi:10.1016/j.tecto.2008.04.014.

López-Escobar, L., R. Kilian, P. D. Kempton, and M. Tagiri (1993), Petrography and geochemistry of Quaternary rocks from the southern volcanic zone of the Andes between 41°30′ and 46°00′S, Chile, *Rev. Geol. Chile*, *20*, 33–55.

Martin, J. H., S. E. Fitzwater, and R. M. Gordon (1990), Iron deficiency limits phytoplankton growth in Antarctic waters, *Global Biogeochem. Cycles*, *4*, 5–12, doi:10.1029/GB004i001p00005.

Martin-Del Pozzo, A. L., T. González-Morán, R. Espinasa-Pereña, M. A. Butron, and M. Reyes (2008), Characterization of the recent ash emissions at Popocatepetl volcano, Mexico, *J. Volcanol. Geotherm. Res.*, *170*, 61–75, doi:10.1016/j.jvolgeores.2007.09.004.

McConnell, J. R., A. J. Aristarain, J. R. Banta, P. R. Edwards, and J. C. Simões (2007), 20th-Century doubling in dust archived in an Antarctic peninsula ice core parallels climate change and desertification in South America, *Proc. Natl. Acad. Sci. U. S. A.*, *104*, 5743–5748, doi:10.1073/pnas.0607657104.

Mella, M. (2008), *Tese de Doutoramento*, 180. pp., Univ. of Sao Paulo, Brazil.

Naranjo, J. A., and C. R. Stern (1998), Holocene explosive activity of Hudson volcano, southern Andes, *Bull. Volcanol.*, *59*, 291–306, doi:10.1007/s004450050193.

Naranjo, J. A., and C. R. Stern (2004), Holocene tephrochronology of the southernmost part (42°30′–45°S) of the Andean southern volcanic zone, *Rev. Geol. Chile*, *31*, 225–240.

Notsu, K., L. López-Escobar, and N. Onuma (1987), Along-arc variations of Sr-isotope composition in volcanic rocks from the southern Andes, *Geochem. J.*, *21*, 307–313.

Pankhurst, R. J., S. D. Weaver, F. Hervé, and P. Larrondo (1999), Mesozoic–Cenozoic evolution of the North Patagonian Batholith in Aysén, southern Chile, *J. Geol. Soc.*, *156*, 673–694, doi:10.1144/gsjgs.156.4.0673.

Pyle, D. M. (1989), The thickness, volume and grain size of tephra fall deposits, *Bull. Volcanol.*, *51*, 1–15, doi:10.1007/BF01086757.

Pyle, D. M. (1995), Assessment of the minimum volume of tephra fall deposits, *J. Volcanol. Geotherm. Res.*, *69*, 379–382, doi:10.1016/0377-0273(95)00038-0.

Pyle, D. M. (2000), Sizes of volcanic eruptions, in *Encyclopedia of Volcanoes*, edited by H. Sigurdsson, pp. 463–475, Academic, San Diego, Calif.

Rose, W. I., S. Self, P. J. Murrow, C. Bonadonna, A. J. Durant, and G. G. J. Ernst (2008), Nature and significance of small volume fall deposits at composite volcanoes: Insights from the October 14, 1974 Fuego eruption, Guatemala, *Bull. Volcanol.*, *70*, 1043–1067, doi:10.1007/s00445-007-0187-5.

Scasso, R. A., H. Corbella, and P. Tiberi (1994), Sedimentological analysis of the tephra from the 12–15 August 1991 eruption of Hudson volcano, *Bull. Volcanol.*, *56*, 121–132.

Tamic, N., H. Behrens, and F. Holtz (2001), The solubility of H_2O and CO_2 in rhyolitic melts in equilibrium with a mixed CO_2–H_2O fluid phase, *Chem. Geol.*, *174*, 333–347, doi:10.1016/S0009-2541(00)00324-7.

Textor, C., H. F. Graf, M. Herzog, J. M. Oberhuber, W. I. Rose, and G. G. J. Ernst (2006), Volcanic particle aggregation in explosive eruption columns. Part I: Parameterization of the microphysics of hydrometeors and ash, *J. Volcanol. Geotherm. Res.*, *150*, 359–377, doi:10.1016/j.jvolgeores.2005.09.007.

T. A. Mather, N. E. Matthews, D. M. Pyle, and S. F. L. Watt, Department of Earth Sciences, University of Oxford, Parks Road, Oxford OX1 3PR, UK. (Sebastian.Watt@earth.ox.ac.uk)

R. S. Martin, Department of Earth Sciences, University of Cambridge, Downing Street, Cambridge CB2 3EQ, UK.